IEEE Access
Multidisciplinary | Rapid Review | Open Access Journal

Received October 20, 2020, accepted November 16, 2020, date of publication December 1, 2020,
date of current version December 17, 2020.

Digital Object Identifier 10.1109/ACCESS.2020.3041526

An Improved Precise Power Control of Voltage Sensorless-MPC for PWM Rectifiers

XIONG XIAO[1], (Member, IEEE), YUJUAN WU[1], JIANTAO SU[2], YONGJUN ZHANG[1], (Member, IEEE), AND JINGZHI ZHOU[3]

[1]National Engineering Research Center for Advanced Rolling Technology, University of Science and Technology Beijing, Beijing 100083, China
[2]School of Mechanical Engineering, University of Science and Technology Beijing, Beijing 100083, China
[3]Department of Sports Science, Zhejiang University, Hangzhou 310028, China

Corresponding author: Yongjun Zhang (zhangyj@ustb.edu.cn)

This work was supported in part by the National Natural Science Foundation of China under Grant 51907006, and in part by the USTB-NTUT Joint Research Program under Grant 06310059.

ABSTRACT In traditional model predictive control (MPC) methods, the power prediction of the state quantity is not only limited by the measurement of the voltage sensor, but also the open-loop control. In order to boost the overall prediction accuracy without AC voltage sensor, an improved sliding mode estimation-model predictive power precision control strategy without AC voltage sensor was proposed. In this paper, the voltage on the network side is dynamically estimated by using sliding mode sigmoid function, and the system stability is proved by the Lyapunov function. On this basis, the active power and reactive power at time k+2 are calculated through the designed rolling optimization prediction link with feedback correction, aiming to reduce power pulse vibration and accurate prediction. The simulation and experimental results show that the proposed control strategy effectively suppresses the influence of grid-side harmonics on the prediction accuracy and improves the overall of the dynamic and static performance of the system.

INDEX TERMS Model predictive control, sliding mode estimation, voltage sensorless.

I. INTRODUCTION

Owing to the considerable advantages of bidirectional energy flow and adjustable power factor [3], three-phase voltage-type pulse width modulation (PWM) rectifiers have been applied to numerous fields, such as industrial transmission of microgrids, wind energy generation systems, active filtering etc. [1], [2]. The PWM rectifier is a multivariable multi-coupling system. In order to improve the performance of the system, vast quantities of advanced control strategies have been applied to system response, parameter identification, coordinated control, and switch control [4]. Model predictive control (MPC) has become a frontier research direction in rectifier control strategies due to its advantages of simple design and easy engineering implementation, especially in dealing with constrained optimization problems in nonlinear systems. Kouro *et al.* [6] compared the MPC with the classic double closed-loop proportion integration (PI) control, which embodies the straightforward structure and high dynamic performance of the MPC controller.

In power electronics, the model predictive direct power control (MPDPC) operates the position of the switch and formulates the control problem as a reference value tracking problem both directly [5], which is one of the most widely used control methods. In order to solve the slow dynamic response and large pulse vibration in the rectifier vector control problem, He *et al.* [3] applied MPC to the active front rectifier for the first time to form MPDPC, which effectively suppressed the DPC power pulse vibration. The MPC was also employed to the inverter side to form MPDTC, which effectively improved the torque pulse [7], [8]. Additionally, MPC has been applied to five-phase PMSM and dual-motor five-bridge arms to reduce torque pulse vibration [9], [10]. It was also applied to both sides of AC-DC-AC to suppress the dynamic voltage fluctuation on the DC bus [11], [12]. The above works suggest that MPC is extensively used.

Meanwhile, many researchers have proposed improved algorithms for MPDPC. For example, new strategies such as multi-step prediction [3], [13], extrapolation [14], and vector angle compensation method are used to avoid the delay of action caused by extensive calculations. Young *et al.* [15] analyzed the influence of model parameter uncertainty on FCS-MPC of a three-phase two-level inverter. Rodriguez and Cortes [17] summarized and optimized the design and parameter selection of the cost function for MPDPC. Geyer [18] derived and visualized the explicit state feedback control

The associate editor coordinating the review of this manuscript and approving it for publication was Alfeu J. Sguarezi Filho.

law of the electric drive model predictive controller. Zhang and Xie [19], Zhang and Yang [20] proposed double-vector and three-vector MPDPC based on a single vector approach and optimized the duty cycle [21].

The above improvements are all aimed at the optimization of MPDPC, improving the performance of the system to a certain extent. However, the control strategy is not changed. Due to voltage sensors, the MPDPC based on grid voltage orientation is inevitably affected by the grid side harmonics. Although vector control (traditional voltage sensorless control [22]) can effectively suppress the above effects [23], DC offset and initial value in virtual flux estimation greatly affect the accuracy of power calculation [24]. Thus, it is of great significance to study MPDPC without grid side voltage sensor based on grid voltage orientation. In the traditional voltage sensorless MPDPC, however, the high-frequency interference is easily introduced due to the current differential voltage estimation component. The primary problem to be solved in the MPDPC without voltage sensor has come to effectively estimate the grid side voltage. Moreover, for MPDPC algorithm, the MPDPC is based on the open-loop prediction of rolling calculation of invariant model. Therefore, it is impossible to fully comply with the actual situation or compensate for the prediction error caused by the change of the set value itself. Steady-state power pulsations caused by constant value changes are inevitable. Therefore, implementing closed-loop MPDPC prediction is key to accurate power prediction.

Since sliding mode control (SMC) does not depend on system parameters, it has strong robustness to unknown parameter variations and noise. The design is simple and easy to implement. Our research group first employed a sliding mode observer to estimate the virtual flux linkage on the rectifier side for the first time [24]. Literature [25] combines a fractional-order SMC method with a recurrent neural network structure to improve the robustness of the system to a certain extent, but the switch function sign used by the observer is prone to high-frequency oscillations. A method combining dynamic sliding mode and terminal sliding mode is proposed to solve the chattering phenomenon in traditional SMC [26]. However, the addition of an integral term in the text increases the complexity of the calculation. The chattering problem of control input can be effectively solved by using the super-twisting algorithm, which makes the control input smoother [27]. But the sliding mode surface contains multiple parameters, and the method integrates multiple algorithms, resulting in a more complex theoretical structure. Researches [28] and [29] combined the sliding mode observer with MPC, resulting in high-frequency oscillations in the system. In addition, these MPC algorithms are established based on open-loop prediction, which indicates that the accuracy of power prediction needs to be improved.

According to the above analysis, this paper applies a simple sliding mode observer to the estimation of the voltage on the grid side of PWM rectifier and combines it with MPC. These approaches verify the feasibility of combining sliding mode estimation with MPC, realize real-time identification of parameters on the rectifier side and precise control of power, and improve the overall prediction accuracy. Meanwhile, a rolling optimization prediction link with feedback correction is designed to further reduce power pulse vibration and improve prediction accuracy.

The current status of the MPDPC search is introduced in Section I, and the existing problems are summarized. Section II constructs a sliding mode voltage observer, using the MPC algorithm to make discrete estimates and realize power prediction. Section III describes the precise prediction based on the sliding mode estimation-model and optimized the predicted power, stating the comprehensive control strategy. Section IV shows the simulation results and experimental results conducted by the MATLAB/Simulink and rectifier-inverter test platform. Finally, the conclusions are drawn in Section V.

II. SLIDING MODE ESTIMATION-MODEL PREDICTIVE POWER CONTROL

In the model prediction power control, the power prediction depends on the prediction of the voltage and current at the next moment, where a voltage sensor generally measures the grid-side voltage. There is less research on model predictive control without voltage sensor. In traditional voltage sensorless PWM rectifiers control, high-frequency interference is easily introduced due to the current differential voltage estimation component. Moreover, the strategy itself is seriously affected by the inductance voltage drop at high frequency. In order to solve the above problems, a voltage sensorless model predictive power control strategy is proposed. In this paper, the sliding mode observer is firstly established to estimate the voltage on the grid side, and the Lyapunov function is used to prove the system stability. Combining with the MPC algorithm, discrete estimation, and power prediction are implemented further for improved performance.

A. GRID SIDE VOLTAGE ESTIMATION UNDER SLIDING MODE OBSERVER

Traditional voltage sensorless DPC and MPC algorithms can be seen in [11] and [22]. According to the basic theory of sliding mode variable structure control and the mathematical model of three-phase PWM rectifiers in stationary coordinates, the sliding mode observer is constructed according to:

$$\begin{pmatrix} L_g \dfrac{d\hat{i}_\alpha}{dt} \\ L_g \dfrac{d\hat{i}_\beta}{dt} \end{pmatrix} = \begin{pmatrix} u_\alpha(t) \\ u_\beta(t) \end{pmatrix} - R \begin{pmatrix} \hat{i}_\alpha \\ \hat{i}_\beta \end{pmatrix} - \begin{pmatrix} u_{g\alpha} \\ u_{g\beta} \end{pmatrix} \tag{1}$$

In Eq. (1), $u_\alpha(t)$, $u_\beta(t)$, $\hat{i}_\alpha$ and $\hat{i}_\beta$ are net side phase voltage and the estimated values of net side input current under $\alpha\beta$ coordinate system, L_g is the inductance value of the net side filter reactance, R_g is the total impedance of the bridge circuit, and $u_{g\alpha}$ and $u_{g\beta}$ are the input phase voltages of the rectifier.

The design of sliding mode voltage observer includes selection of switching function and construction of sliding

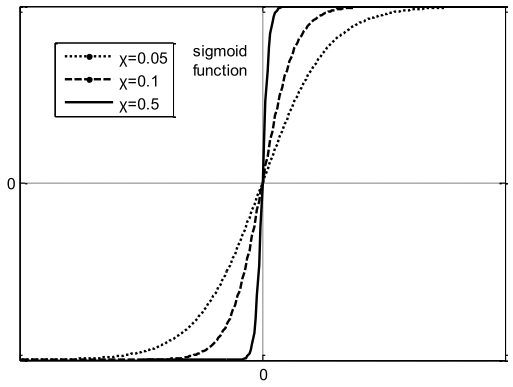

FIGURE 1. Curve of *S* functions.

mode voltage observer model. The design of sliding mode observer used in this paper has been proposed in [24].

The selection of the switching function is the key to design the sliding mode voltage observer. The sliding mode observer designed with the traditional sign switching function suffered from high-frequency system chattering and increased voltage fluctuation on the DC side. In order to reduce the high frequency chattering of the system, a new sigmoid (S) function is proposed from the perspective of boundary layer continuous control to replace the traditional sign function. The S function is expressed as:

$$\begin{bmatrix} S\left(\bar{i}_\alpha\right) \\ S\left(\bar{i}_\beta\right) \end{bmatrix} = \begin{bmatrix} \left(\dfrac{2}{1+e^{-\chi \bar{i}_\alpha}}\right) - 1 \\ \left(\dfrac{2}{1+e^{-\chi \bar{i}_\beta}}\right) - 1 \end{bmatrix} \tag{2}$$

where, χ is a constant used to adjust the slope. Fig. 1 shows the S function curve under various χ values.

The error in stator current estimation is defined as: $\bar{i}_\alpha = \hat{i}_\alpha - i_\alpha$ and $\bar{i}_\beta = \hat{i}_\beta - i_\beta$, i_α and i_β are measured values of net side incoming current.

The grid voltage estimate can be expressed as:

$$\begin{cases} u_\alpha(t) = KS\left(i_\alpha - \hat{i}_\alpha\right) \\ u_\beta(t) = KS\left(i_\beta - \hat{i}_\beta\right) \end{cases} \tag{3}$$

where, K is the sliding mode gain.

The dynamic error equation obtained by (1) and (3), it can be derived as:

$$\begin{pmatrix} \dfrac{\mathrm{d}\left(\bar{i}_\alpha\right)}{\mathrm{d}t} \\ \dfrac{\mathrm{d}\left(\bar{i}_\beta\right)}{\mathrm{d}t} \end{pmatrix} = -\frac{1}{L_g}\begin{pmatrix} u_\alpha \\ u_\beta \end{pmatrix} - \frac{R_g}{L_g}\begin{pmatrix} \bar{i}_\alpha \\ \bar{i}_\beta \end{pmatrix} + \frac{1}{L_g}\begin{pmatrix} KS\left(\bar{i}_\alpha\right) \\ KS\left(\bar{i}_\beta\right) \end{pmatrix} \tag{4}$$

When the system reaches sliding mode operation, it can be derived as:

$$\begin{cases} \dfrac{\mathrm{d}\left(\bar{i}_\alpha\right)}{\mathrm{d}t} = \hat{i}_\alpha - i_\alpha = 0 \\ \dfrac{\mathrm{d}\left(\bar{i}_\beta\right)}{\mathrm{d}t} = \hat{i}_\beta - i_\beta = 0 \end{cases} \tag{5}$$

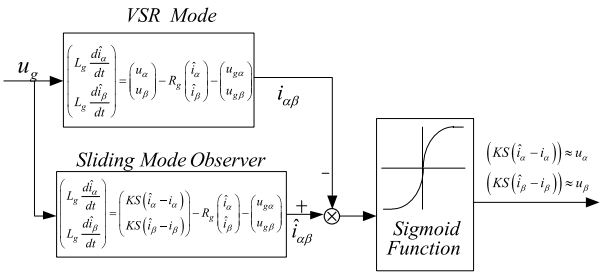

FIGURE 2. Diagram of sliding mode observer.

According to the above equation, the grid voltage can be expressed as:

$$\begin{aligned} KS\left(i_\alpha - \hat{i}_\alpha\right) &\approx u_\alpha \\ KS\left(i_\beta - \hat{i}_\beta\right) &\approx u_\beta \end{aligned} \tag{6}$$

The sliding mode observer (SMO) structure is shown in Fig 2.

B. STABILITY PROOF AND COMPREHENSIVE CONTROL STRATEGY

To prove its stability, a Lyapunov function is established as:

$$V = \frac{1}{2} S_n^T S_n \tag{7}$$

If it is stable, then

$$\dot{V} = S_n^T \dot{S}_n \tag{8}$$

where

$$S_n = \begin{bmatrix} S_\alpha & S_\beta \end{bmatrix}^T = \begin{bmatrix} \hat{i}_\alpha - i_\alpha & \hat{i}_\beta - i_\beta \end{bmatrix}^T \tag{9}$$

and

$$\dot{S}_n = \begin{bmatrix} \dot{S}_\alpha & \dot{S}_\beta \end{bmatrix}^T = \begin{bmatrix} \dot{\hat{i}}_\alpha - \dot{i}_\alpha & \dot{\hat{i}}_\beta - \dot{i}_\beta \end{bmatrix}^T \tag{10}$$

Combining (1), (4) and (8), the Lyapunov function can be formulated according to:

$$\begin{aligned} \dot{V} &= S_n^T \dot{S}_n = S_\alpha \dot{S}_\alpha + S_\beta \dot{S}_\beta \\ &= -\frac{R_g}{L_g}\left[\left(\hat{i}_\alpha - i_\alpha\right)^2 + \left(\hat{i}_\beta - i_\beta\right)^2\right] \\ &\quad -\frac{1}{L_g}\left[\left(\hat{i}_\alpha - i_\alpha\right)u_\alpha - \left(\hat{i}_\alpha - i_\alpha\right)KS\left(\hat{i}_\alpha - i_\alpha\right)\right] \\ &\quad -\frac{1}{L_g}\left[\left(\hat{i}_\beta - i_\beta\right)u_\beta - \left(\hat{i}_\beta - i_\beta\right)KS\left(\hat{i}_\beta - i_\beta\right)\right] \le 0 \end{aligned} \tag{11}$$

The conditional expression (11) is satisfied so that a minimum value sufficiently smaller than negative can be obtained.

$$K = u_{\max}\left(\frac{e^{-\chi \bar{i}_{\max}} + 1}{e^{-\chi \bar{i}_{\max}} - 1}\right) \tag{12}$$

If (12) is satisfied, then $\dot{V} < 0$, and the SMO will converge regardless of the equivalent resistance and inductance values.

C. FINAL SLIDING MODE ESTIMATION-MODEL PREDICTIVE POWER CONTROL

The combined sliding mode observer estimation with MPC control requires redefining the active power and reactive power prediction values. In order to cooperate with digital signal processing, the discrete system used in MPC employs discrete-time sliding mode estimation. The observer obtains input values at each sampling period, and the input values remain unchanged during the interval.

Equation (4) can be discretized, and the dynamic error equation at time $k+1$ is given by:

$$\begin{pmatrix} L_g \dfrac{\bar{i}_\alpha(k+1)-\bar{i}_\alpha(k)}{T_s} \\ L_g \dfrac{\bar{i}_\beta(k+1)-\bar{i}_\beta(k)}{T_s} \end{pmatrix} = -\frac{1}{L_g}\begin{pmatrix} u_\alpha(k) \\ u_\beta(k) \end{pmatrix} - \frac{R_g}{L_g}\begin{pmatrix} \bar{i}_\alpha(k) \\ \bar{i}_\beta(k) \end{pmatrix} + \frac{1}{L_g}\begin{pmatrix} KS\left(\bar{i}_\alpha(k)\right) \\ KS\left(\bar{i}_\beta(k)\right) \end{pmatrix} \tag{13}$$

when the system reaches the sliding mode operation, the grid side voltage estimate can be expressed as:

$$\begin{cases} u_\alpha(k) = KS\left(\bar{i}_\alpha(k)\right) \\ u_\beta(k) = KS\left(\bar{i}_\beta(k)\right) \end{cases} \tag{14}$$

According to the instantaneous power principle, the predicted expression of instantaneous active power and reactive power at time $k+1$ is

$$\begin{cases} P(k+1) = \mathrm{Re}\left\{KS\left(\overline{\mathbf{i}_g}(k+1)\right)\overline{\mathbf{i}_g}(k+1)\right\} \\ Q(k+1) = \mathrm{Im}\left\{KS\left(\overline{\mathbf{i}_g}(k+1)\right)\overline{\mathbf{i}_g}(k+1)\right\} \end{cases} \tag{15}$$

III. ACCURATE PREDICTION OPTIMIZATIONS BASED ON ESMO-DPC

A. ERROR FEEDBACK CORRECTION DESIGN BASED ON MULTI-STEP PREDICTION

In Sections II, the MPC conducts prediction based on the invariant model. Thus it is impossible to fully comply with the actual situation. Firstly, it does not compensate for the prediction error caused by the change of the set value itself. Moreover, steady-state power pulsation is also inevitable. Feedback plays an irreplaceable role in overcoming the influence of interference, uncertainty, and obtaining closed-loop stability. Based on predictive power control with the sliding mode voltage estimation model (SMO-MPDPC), this paper introduces feedback correction to reduce the error caused by the change of set value in the actual prediction process. Based on the predicted output of the model, the predicted value is continuously corrected according to the actual output of the system, and then new optimization is performed.

The definition of $e(k+1)$ is the difference between the actual state variable value and the predicted value at the $k+1$ time step; it can be derived as:

$$e(k+1) = X(k+1) - X^m(k+1|k) \tag{16}$$

where $X(k+1)$ is the feedback value at time $k+1$, and $X^m(k+1)$ indicates the predicted value at time $k+1$. Since $X(k+1)$ is not available, the approximate representation $e(k)$ is used for $e(k+1)$ given by:

$$e(k) = X(k) - X^m(k|k-1) \tag{17}$$

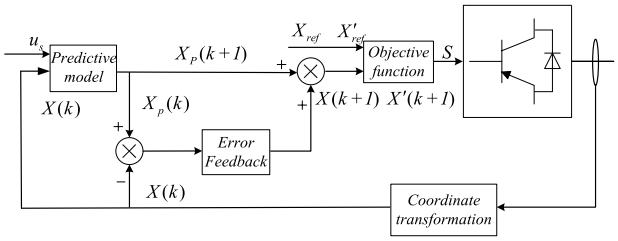

FIGURE 3. Error feedback correction structure diagram.

The corrected prediction value can be calculated by adding the error to the prediction output of the model:

$$X^p(k+1) = X^m(k+1|k) + h_p e(k) \tag{18}$$

where h_p is the error compensation factor, and its structure is shown in Fig 3.

Then the power prediction can be expressed as:

$$\begin{pmatrix} P^p(k+1) \\ Q^p(k+1) \end{pmatrix} = \begin{pmatrix} P^m(k+1|k) \\ Q^m(k+1|k) \end{pmatrix} + h_p\begin{pmatrix} P^p(k)-P(k) \\ Q^p(k)-Q(k) \end{pmatrix} \tag{19}$$

In Eq. (19), $P^p(k+1)$ and $Q^p(k+1)$ indicate the predicted values of the active and reactive power corrected by the feedback at time $k+1$, respectively. $P^p(k)$ and $Q^p(k)$ represent the corresponding values at the time k. $P^m(k+1)$ and $Q^m(k+1)$ denote the predicted values of the active power and the reactive power obtained according to the discrete model at time $k+1$, respectively. $P^p(k)$ and $Q^p(k)$ are the actual feedback of the active power and the reactive power at time k, respectively. In order to reduce the number of simulations, a branch and bound principle can be used to determine the error compensation factor h_p, according to the actual situation of the system.

B. COMPREHENSIVE CONTROL AFTER DELAY COMPENSATION

Considering that there is control delay in the actual control system. The delay compensation control amount can formulated subject to (19) as:

$$\begin{pmatrix} P^p(k+2) \\ Q^p(k+2) \end{pmatrix} = \begin{pmatrix} P^m(k+2|k+1) \\ Q^m(k+2|k+1) \end{pmatrix} + h_p\begin{pmatrix} P^p(k+1)-P(k+1) \\ Q^p(k+1)-Q(k+1) \end{pmatrix} \tag{20}$$

According to (15), it can be derived as:

$$\begin{cases} P^m(k+2|k+1) = \mathrm{Re}\left\{KS\left(\overline{\mathbf{i}_g}(k+2)\right)\overline{\mathbf{i}_g}(k+2)\right\} \\ Q^m(k+2|k+1) = \mathrm{Im}\left\{KS\left(\overline{\mathbf{i}_g}(k+2)\right)\overline{\mathbf{i}_g}(k+2)\right\} \end{cases} \tag{21}$$

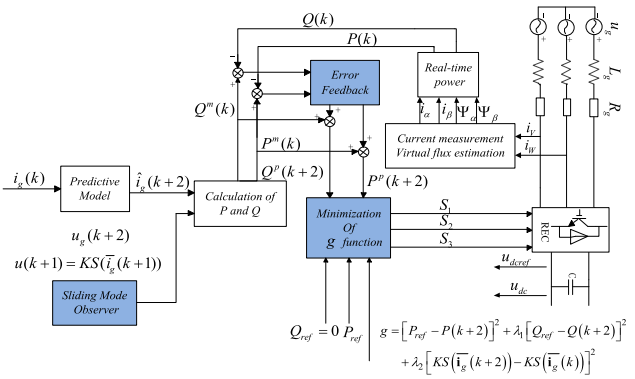

FIGURE 4. Diagram of SMO-MPDPC structure.

Combined with (19), the final active and reactive power expressions are formulated as:

$$\begin{aligned}\begin{pmatrix} P^p(k+2) \\ Q^p(k+2) \end{pmatrix} &= \begin{pmatrix} \mathrm{Re}\left\{KS\left(\overline{\mathbf{i}}_g(k+2)\right)\overline{\mathbf{i}}_g(k+2)\right\} \\ \mathrm{Im}\left\{KS\left(\overline{\mathbf{i}}_g(k+2)\right)\overline{\mathbf{i}}_g(k+2)\right\} \end{pmatrix} \\ &+ h_p \begin{pmatrix} \mathrm{Re}\left\{KS\left(\overline{\mathbf{i}}_g(k+1)\right)\overline{\mathbf{i}}_g(k+1)\right\} \\ \mathrm{Im}\left\{KS\left(\overline{\mathbf{i}}_g(k+1)\right)\overline{\mathbf{i}}_g(k+1)\right\} \end{pmatrix} \\ &+ h_p^2 \begin{pmatrix} P^p(k) \\ Q^p(k) \end{pmatrix} - h_p \begin{pmatrix} P(k+1) \\ Q(k+1) \end{pmatrix} - h_p^2 \begin{pmatrix} P(k) \\ Q(k) \end{pmatrix} \end{aligned} \tag{22}$$

C. OBJECTIVE FUNCTION OPTIMIZATION DESIGN

In the voltage estimation, the prediction error of the switching function and current should be considered. The prediction error of the current has a power term limitation in the objective function. Therefore, considering the influence of the voltage prediction error and increasing the voltage estimation limit, the optimized objective function can be selected as:

$$\begin{aligned} g = &\left[P_{ref} - P(k+2)\right]^2 + \lambda_1 \left[Q_{ref} - Q(k+2)\right]^2 \\ &+\lambda_2 \left[KS\left(\overline{\mathbf{i}}_g(k+2)\right) - KS\left(\overline{\mathbf{i}}_g(k)\right)\right]^2 \end{aligned} \tag{23}$$

In Eq. (23), λ_1 and λ_2 are the weight of reactive power and switching function, respectively. The root mean square (RMS) of the current tracking error and the voltage estimation error is defined as the evaluation function index of λ_1 and λ_2 regulation effect. The locking range is used to select λ_1 and λ_2 according to the branch and bound principle. The final value is determined according to the variation of the random value of the active power and the load current.

Finally, the sliding mode estimation-MPDPC structure diagram is shown in Fig. 4.

IV. SIMULATION AND EXPERIMENT

A. SYSTEM SIMULATION

The simulation model was built in MATLAB/Simulink, and the simulations results were compared with the four control methods, which are voltage sensorless DPC under vector control (TDPC), DPC with sliding mode voltage estimation (SMO-DPC), predictive power control with sliding mode voltage estimation model (SMO-MPDPC) and sliding mode voltage estimation model predictive power control with error feedback correction (ESMO-MPDPC). Parameters used in the following simulations are shown in Table 1, including main parameters and control parameters under four different strategies.

TABLE 1. System Parameters.

Model Parameters		H_p/Active power hysteresis	200 W
Symbol/Parameters	Value	H_q/Reactive power hysteresis	100 Var
u_{abc}/Grid power phase voltage	220 V	K/Slip gain factor	-320
f_n/Grid voltage frequency	50 HZ	**SMO-MPDPC**	
u_{dc}/Bus voltage	520 V	K_p/Proportional gain	0.5
L_g/AC side input inductor	5.5 mH	K_i/Integral Gain	5
R_g/AC side resistor	15 mΩ	K/Slip gain factor	-320
C_{dc}/DC side filter capacitor	2200 μF	ω/Grid base wave angle frequency	10^4 rad/s
R_{dc}/Load resistance	30 Ω	λ_1/Weight factor for reactive power	0.1
T_s/Sampling period	4e-5s	χ/Adjustment coefficient of S function	1
TDPC		**ESMO-MPDPC**	
K_p/Proportional gain	0.5	K_p/Proportional gain	0.5
K_i/Integral Gain	5	K_i/Integral Gain	5
H_p/Active power hysteresis	200 W	K/Slip gain factor	-320
H_q/Reactive power hysteresis	100 Var	ω/Grid base wave angle frequency	10^4 rad/s
SMO-DPC		λ_1/Reactive power weight factor	0.1
K_p/Proportional gain	0.5	λ_2/Switch function weight factor	0.3
K_i/Integral Gain	5	h_p/Error feedback factor	0.8
χ/Adjustment coefficient of S function	1	χ/Adjustment coefficient of S function	1

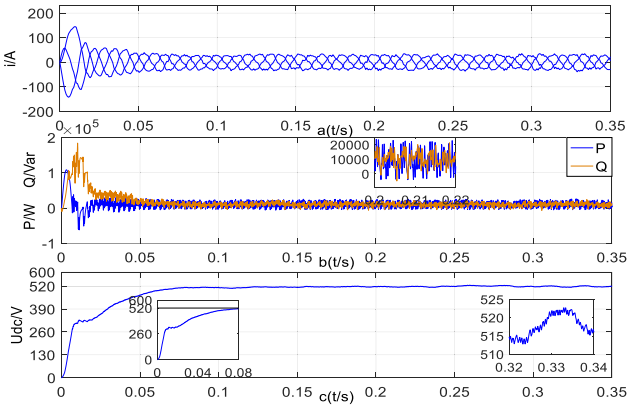

FIGURE 5. Waveform diagram of startup and Steady State Simulation based on direct power control of traditional voltage sensorless.

Fig. 5 shows the simulations of grid-side current (i), active power (P) and reactive power (Q) and DC bus voltage (u_{dc}) for TDPC startup and steady state, respectively. The fluctuation range is between ±150A of grid-side current. The time to reach the steady state is 0.05 s, and the harmonic is seriously affected at steady state. The current value shows non-standard sine waves with fluctuation. Due to the logic switch table used, there are some areas of reactive power regulation with large fluctuations. The active power and reactive power pulse vibration is large (about 30 kW/20 kVar), and the system is not operating at unit power factor. The DC bus voltage has a large fluctuation during startup, and the rising time of the

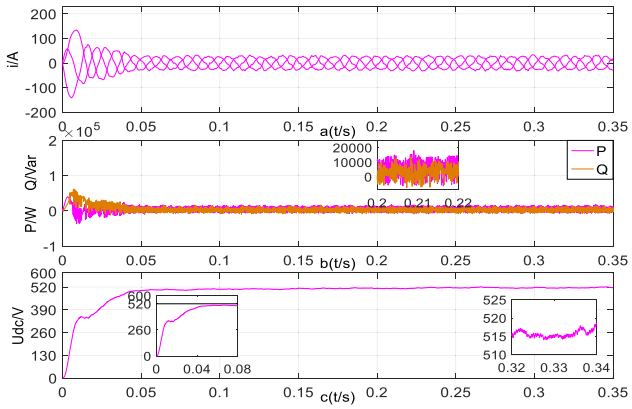

FIGURE 6. Sliding mode estimation direct power control startup and steady state simulation waveform diagram.

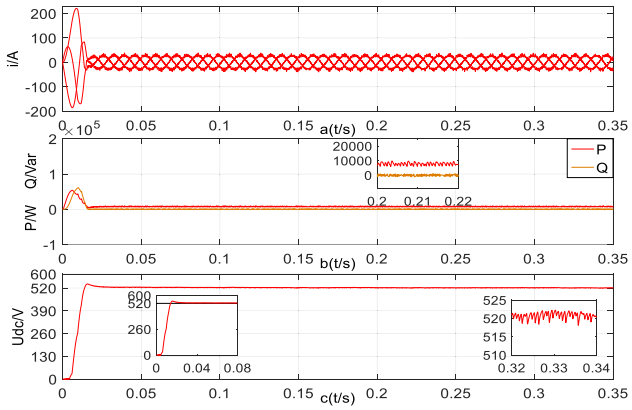

FIGURE 7. Sliding mode estimation waveform diagram at startup and steady state simulation based on model predictive control.

bus voltage is slow (0.25 s). The fluctuation is relatively large when reaching the steady state, the fluctuation is 10 V and the pulse vibration is about 4 V.

Fig. 6 is a waveform diagram of startup and steady-state simulation based on SMO-DPC, corresponding to waveforms Fig. 5, respectively. Due to the presence of harmonics, sine wave still exists in AC side current at steady state. The rising time at startup is reduced to 0.04 s and the fluctuation range is between ± 140 A. The active power and reactive power pulsation reach 21 kW/15 kVar. The DC bus voltage still fluctuates at startup, and the rising time of the bus voltage is 0.25 s. When it reaches steady state, the fluctuation is about 6 V and the pulse vibration is 3 V.

In order to solve the pulse vibration problem of DPC and achieve precise control, the two-step model is used to predict SMO-MPDPC. Fig. 7 shows the startup and steady-state simulation waveforms of SMO-MPDPC. The AC side current fluctuates greatly at the beginning, but the steady state can be reached within 0.02 s. The waveform stability of active power and reactive power also greatly improved. Compared with SMO-DPC, the fluctuation at startup is small. The pulse vibration can be maintained within 4 kW/2 kVar at steady state. Moreover, the system is operating at unit power factor. The DC bus voltage value is stable and the pulsation is 3 V. The rising time at startup is 0.2 s with a peak value of 543 V.

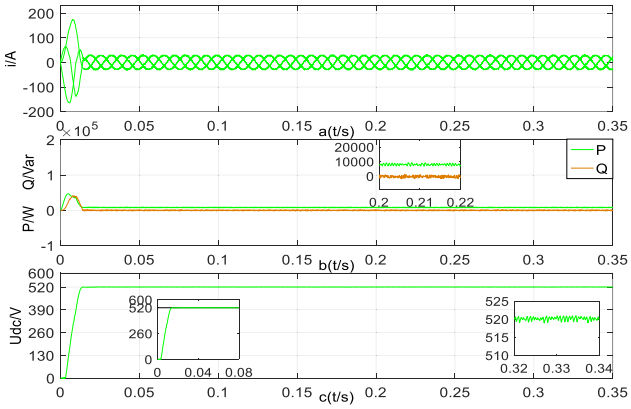

FIGURE 8. Sliding mode estimation with error feedback startup and steady state simulation waveforms based on model predictive control.

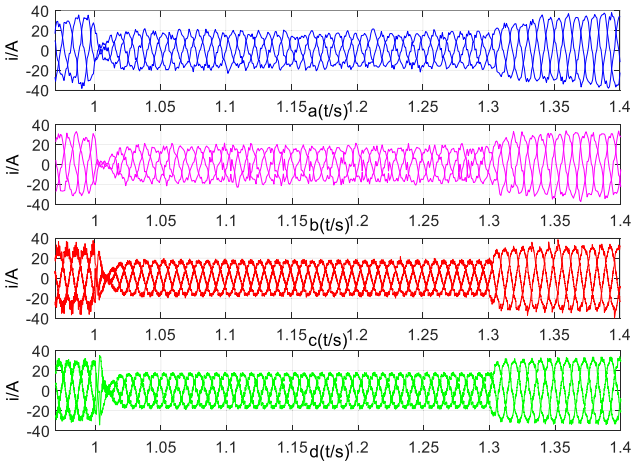

FIGURE 9. Simulation waveform diagram of AC side current in step response of bus voltage set point and load change response.

Fig. 8 shows the startup and steady-state simulation waveforms of ESMO-MPDPC. The error feedback correction is used to compensate for the prediction error, which improves the overall prediction accuracy. The fluctuation of the grid side current within ±150 A at starting moment. The steady state is reached at 0.02 s with a standard sine current waveform. The pulsation of power is within 2 kW/2.5 kVar. There is no overshoot when the DC bus voltage starts, and it only takes 0.015 s to reach the steady state time with a pulsation range of 2 V.

Figs. 9-12 show the three-phase current (i) comparison diagram, active power (P) and reactive power (Q) comparison diagram, bus voltage (u_{dc}) comparison diagram, and grid side voltage u_α of the four methods under dynamic step inputs. The bus voltage setting at 1s is 520 V step to 400 V, and a 30 Ω load is connected in parallel at 1.3 s, where a-d represents the simulation waveforms of TDPC, SMO-DPC, SMO-MPDPC, and ESMO-MPDPC, respectively.

The simulation comparison analysis data based on the four control strategies is shown in Table 2. The error of TDPC estimation for u_α is relatively large. It has weak interference capability and poor robustness. After adding the sliding mode

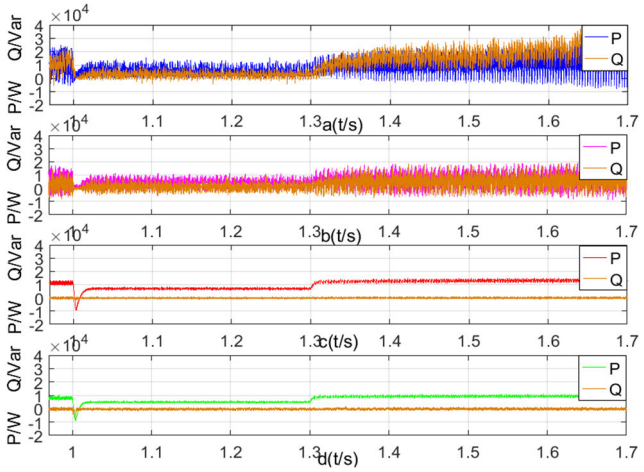

FIGURE 10. Simulation waveform of active power and reactive power in step response of bus voltage set point and load change response.

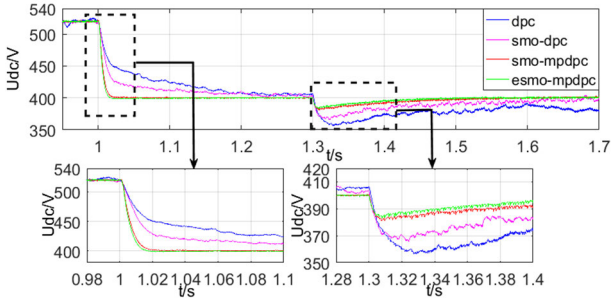

FIGURE 11. Simulation waveform of DC bus voltage in step response of bus voltage set point and load change response.

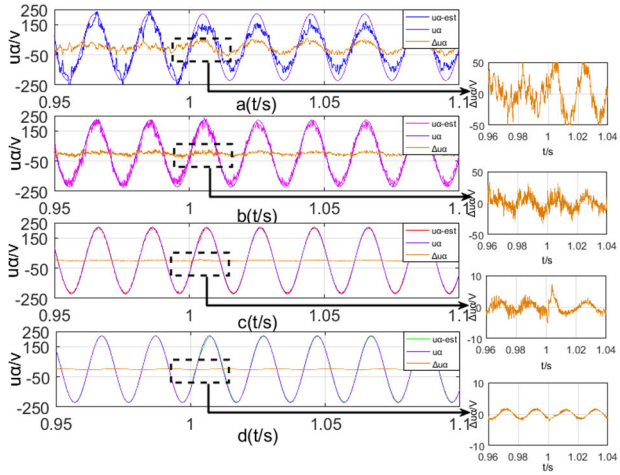

FIGURE 12. Simulation waveform of actual grid voltage, estimated grid voltage and estimated error in step response of bus voltage set point.

estimation, the error is reduced, it has a faster response time, shorter convergence time and less fluctuation. However, the anti-interference ability still cannot meet industrial requirements. SMO-MPDPC can respond quickly, and the convergence time is short. The fluctuation of bus voltage and active power under disturbance is small. After adding the power error feedback, the estimated voltage and the actual

TABLE 2. Simulation data comparison for different methods.

	TDPC	SMO-DPC	SMO-MPDPC	ESMO-MPDPC
u_α Estimated error (Bus voltage step)	50 V	40 V	10 V	2 V
u_{dc} Convergence time (Bus voltage step)	0.4 s	0.3 s	0.04 s	0.01 s
u_{dc} Fluctuation (Load mutation)	43 V	35 V	20 V	18 V
u_{dc} Convergence time (Load mutation)	0.6 s	0.4 s	0.26 s	0.2 s
PQ Fluctuation (Bus voltage step)	29 kW /25 kVar	20 kW /15 kVar	17 kW /6 kVar	15 kW /6 kVar
PQ Convergence time (Load mutation)	0.35 s	0.11 s	0.02 s	0.02 s
i Convergence time (Bus voltage step)	0.03 s	0.03 s	0.02 s	0.02 s
i Response time (Load mutation)	0.01 s	0.01 s	0 s	0 s
i Convergence time (Load mutation)	0.34 s	0.11 s	0.02 s	0.02 s

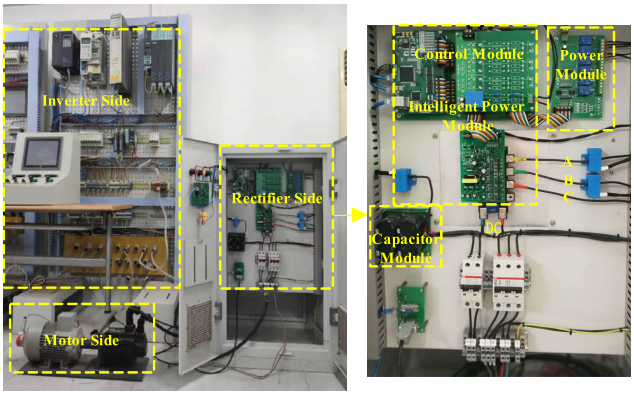

FIGURE 13. Experimental platform.

voltage are basically coincident. It can solve the problems of pulse vibration, jitter and harmonics and reduce high frequency interference. The system still maintains characters of short response time, high prediction accuracy and fast tracking speed under interference.

B. EXPERIMENTAL VERIFICATION

The ESMO-MPDPC strategy is verified experimentally on a self-developed rectifier-inverter platform. Fig.13 is a photograph of the experimental prototype controller and the load motor. The main loop of the system adopts a voltage-type AC-DC-AC topology, and the load of the system is composed of a motor supporting structure consisting of an asynchronous motor of model 1LA7096-4A10-Z and a permanent magnet synchronous motor of model 1FT6. The control platform uses a high-speed digital signal processor (DSP) TMS320F28335 to complete the control algorithm and PWM pulse calculation, and a field programmable gate array (FPGA) to complete the distributed collection of control data and hardware protection. The control part is mainly composed of the rectifier side and the inverter side, and both sides are composed of three IGBT bridge arms. The rectification control employs a PWM pulse rectification to realize four-quadrant rectification. The rectifier side includes a capacitor module, an intelligent power module, a control module, and a power module.

TABLE 3. System Parameters.

Main Parameters of Motor		R_r/Rotor resistance	1.85681 Ω
P_n/Rated Power	2.2 kW	L_r/Rotor inductor	12.65 mH
V_n/Rated rus voltage	400 V	L_m/Mutual inductance	0.3 H
R_s/Stator resistance	3.1 Ω	p/Polar number	2
L_s/Statin inductor	12.65 mH	J/Inertia	0.1 kg·m²
f/Rectifier switch frequency	25 kHZ	T_m/Rated torque	28 N·m
K_i/Integral Gain	1.5	h_p/Error feedback factor	0.8

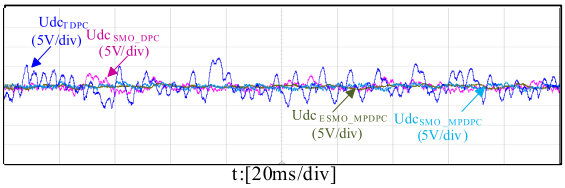

FIGURE 14. DC bus voltage at steady state.

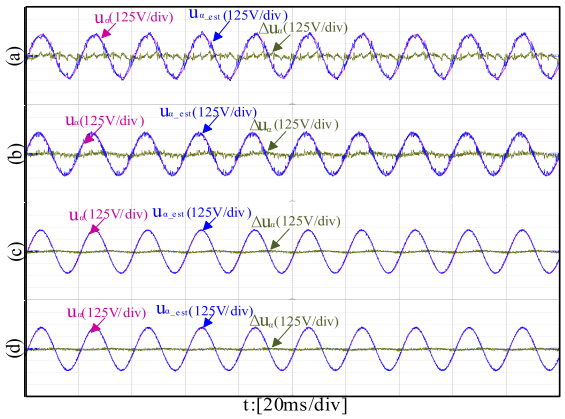

FIGURE 15. u_α, estimated grid voltage u_{α_eat}, and estimation error Δu_α.

Based on the fast bus technology, the system can achieve high-performance motor vector control, motor model optimization, motor parameter automatic identification and other functions. The main parameters of the experimental device are the same as the simulation. The inverter side is controlled by MPDTC and an asynchronous motor is used in the experiment. The main parameters of motor are shown in Table. 3.

Fig. 14 is a waveform diagram of the DC side bus voltage at steady state based on the four control modes. It can be seen that the pulse vibration of TDPC in steady state is more serious, and the pulse vibration range is within 10V. After adding a sliding mode observer, the pulse vibration is obviously suppressed, and the SMO-DPC is controlled within 4V. The SMO-MPDPC control strategy further improves the steady-state DC bus voltage waveform based on the SMO-DPC strategy, and the pulse vibration range is less than 2V. The pulse vibration under the ESMO-MPDPC control strategy is only 0.5 V, which is basically eliminated.

Fig. 15 show the grid side voltages, actual grid side voltages, and estimation errors estimated of the α phase by the four control methods in the two-phase stationary $\alpha\beta$ coordinate system. Fig. 16 and Fig. 17 are comparison diagrams of the grid side estimated voltage u_α and the grid side current i_α and the comparison of u_α and u_β

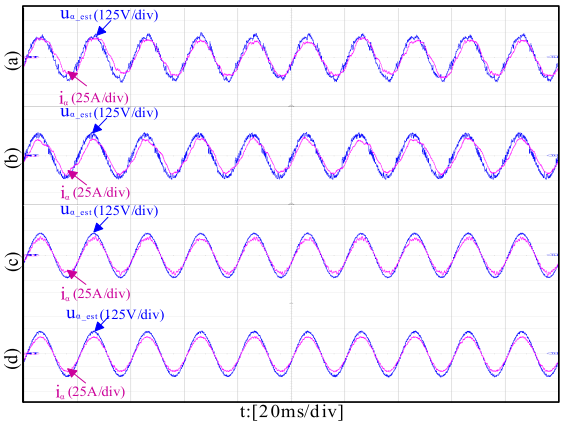

FIGURE 16. Grid side phase voltage u_{α_eat} and phase current i_α.

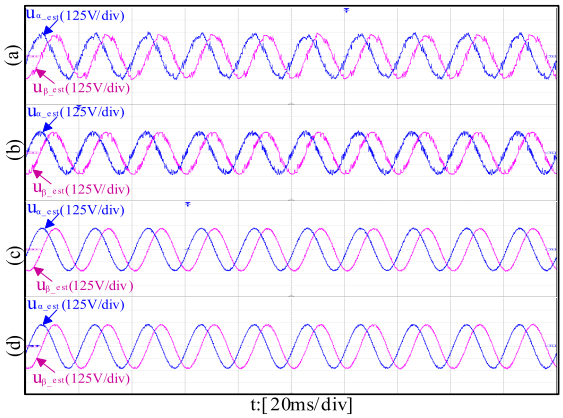

FIGURE 17. Grid side input estimated grid voltage.

after Clark transformation, based on the four control strategies. The value of i_α is magnified by 5 times for clarity. Where panel (a) shows TDPC, diagram (b) shows SMO-DPC, diagram (c) shows SMO-MPDPC, and diagram (d) shows ESMO-MPDPC.

From the comparison of the four control methods in Fig. 15, it can be seen that there is a certain jitter in the grid voltage curve estimated by TDPC. The estimation error is around 50 V. The estimated grid-side voltage under SMO-DPC control is closer to sinusoidal behaviour, and its error is around 50 V. The error is reduced to around 10 V under SMO-MPDPC. When the error feedback is added, the estimated voltage and the actual voltage are basically coincide, with only less than 2 V difference.

It can be seen from Fig. 16 and Fig. 17 that there is a phase difference between voltage and current under TDPC, both current and voltage are non-standard sine waves. The voltage and current fluctuations are relatively large. After adding the sliding mode estimation, although the voltage and current still have a specific phase difference, the sinusoidal and tip fluctuations of the waveform are improved. After adding the sliding mode estimation-model prediction, the estimated jitter of the grid voltage value is substantially eliminated, the influence of harmonics is suppressed, and the phase voltage is in phase with the phase current.

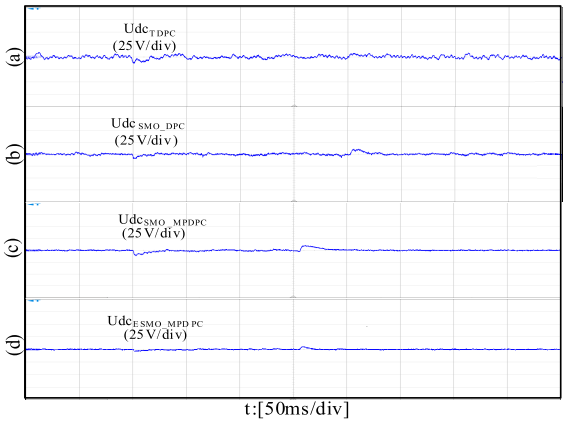

FIGURE 18. DC bus voltage when the speed step.

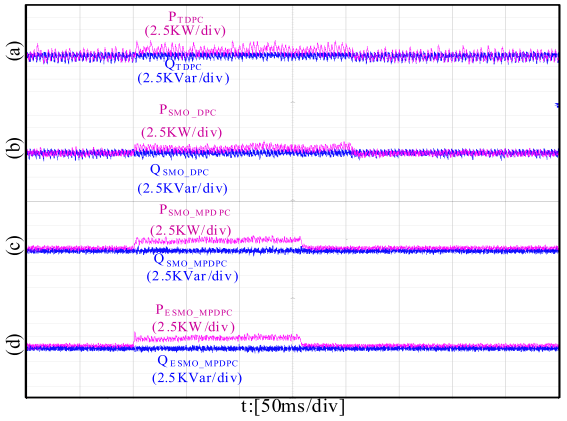

FIGURE 19. Active power and reactive power when speed step.

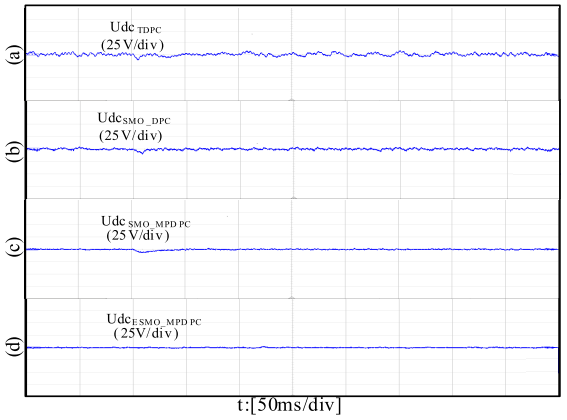

FIGURE 20. DC bus voltage during torque step.

Fig. 18 and Fig. 19 show the comparison of the DC bus voltage, the active power, and reactive power in the four methods under a sudden change in the speed. At 0.6 s, the motor speed increased from 10 rad/s to 30 rad/s. The bus voltage soared (around 13 V) after the sudden change of the motor speed under TDPC, at 0.2 s, the balance is restored, the value of the active power has a large fluctuation (about 2 kW). The SMO-DPC control makes the bus voltage fluctuation smaller, with a maximum fluctuation of 10V and a decrease in the active power of 1.2 kW. The SMO-MPDPC control compared

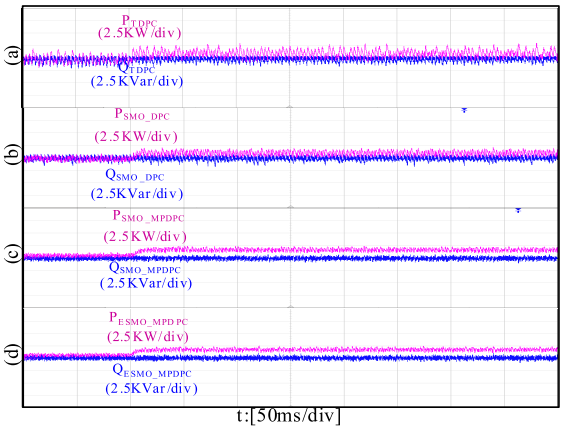

FIGURE 21. Active power and reactive power when torque step.

to the SMO-DPC control significantly improves the dynamic performance of the DC side, the bus voltage converges to equilibrium at 0.17 s, and the power fluctuation is reduced to 0.9 kW. Under the control of ESMO-MPDPC with error feedback correction, the DC voltage fluctuation was further reduced with the maximum value of 4 V, the response speed for the change of speed was accelerated, and the oscillation was eliminated to a certain extent, only 0.5 kW.

Fig. 20 and Fig. 21 are the DC bus voltage comparison diagram and the power comparison diagrams of the four methods under a sudden change of torque. At 1s, the motor torque is increased from 0 N·m to 10 N·m. Based on the four control strategies, the maximum fluctuations of the torque step response are 13 V, 10 V, 6 V and 2 V, respectively. The SMO-MPDPC with error feedback correction almost reached 400 V reference voltage without fluctuation. Response times were 120 ms, 70 ms, 50 ms, and 10 ms, respectively. It can be seen that the addition of the MPC control algorithm with error feedback significantly reduces the response time. Moreover, Fig. 21 indicates that the value of active power under the control of traditional DPC and SMO-DPC increases from 0 kW to 0.5 kW, and it does not work under unit power factor. However, based on SMO-MPDPC and ESMO-MPDPC with error feedback correction, the value of active power is increased by 1 kW from 0 kW and the system operate at unit power factor.

V. CONCLUSION

In this paper, an improved precise power control of voltage sensorless-MPC is proposed based on the direct power control of PWM rectifiers, which integrates sliding mode estimation and error feedback compensation. The simulation and experimentation results show that:

- The sliding mode observer proposed in this paper can track the grid side voltage under dynamic and static conditions in real-time and reduce the estimation error.
- By combining sliding mode estimation with MPDPC was verified, the tracking and prediction of power were realized, and the system response was accelerated.

- The integrated control strategy of closed-loop power error feedback was added to further reduce power pulse and improve prediction accuracy.

The control strategy proposed in this paper can also effectively suppress the fluctuation of DC bus voltage, especially in high-performance applications with load mutation characteristics. It can promote the dynamic and static performance of the system, which shows a great potential in engineering practices.

REFERENCES

[1] P. CortÉs, J. RodrÌguez, P. Antoniewicz, and M. Kazmierkowski, "Direct power control of an AFE using predictive control," *IEEE Trans. Power Electron.*, vol. 23, no. 5, pp. 2516–2523, Sep. 2008.

[2] L. Yin, Z. Zhao, T. Lu, S. Yang, and G. Zou, "An improved DC-link voltage fast control scheme for a PWM rectifier-inverter system," *IEEE Trans. Ind. Appl.*, vol. 50, no. 1, pp. 462–473, Jan. 2014.

[3] H. He, T. Si, L. Sun, B. Liu, and Z. Li, "Linear active disturbance rejection control for three-phase voltage-source PWM rectifier," *IEEE Access*, vol. 8, pp. 45050–45060, 2020.

[4] A. Djerioui, K. Aliouane, and F. Bouchafaa, "Sliding mode direct power control strategy of a power quality based on a sliding mode observer," *Int. J. Electr. Power Energy Syst.*, vol. 56, pp. 325–331, Mar. 2014.

[5] P. Cortés, M. P. Kazmierkowski, R. M. Kennel, D. E. Quevedo, and J. Rodríguez, "Predictive control in power electronics and drives," *IEEE Trans. Ind. Electron.*, vol. 55, no. 12, pp. 4312–4324, Dec. 2008.

[6] S. Kouro, P. Cortes, R. Vargas, U. Ammann, and J. Rodriguez, "Model predictive control—A simple and powerful method to control power converters," *IEEE Trans. Ind. Electron.*, vol. 56, no. 6, pp. 1826–1838, Jun. 2009.

[7] A. A. Ahmed, B. K. Koh, and Y. I. Lee, "A comparison of finite control set and continuous control set model predictive control schemes for speed control of induction motors," *IEEE Trans. Ind. Informat.*, vol. 14, no. 4, pp. 1334–1346, Apr. 2018.

[8] J. Rodriguez, R. M. Kennel, J. R. Espinoza, M. Trincado, C. A. Silva, and C. A. Rojas, "High-performance control strategies for electrical drives: An experimental assessment," *IEEE Trans. Ind. Electron.*, vol. 59, no. 2, pp. 812–820, Feb. 2012.

[9] G. Li, J. Hu, Y. Li, and J. Zhu, "An improved model predictive direct torque control strategy for reducing harmonic currents and torque ripples of five-phase permanent magnet synchronous motors," *IEEE Trans. Ind. Electron.*, vol. 66, no. 8, pp. 5820–5829, Aug. 2019.

[10] Q. Chen, X. Luo, L. Zhang, and S. Quan, "Model predictive control for three-phase four-leg grid-tied inverters," *IEEE Access*, vol. 5, pp. 2834–2841, 2017.

[11] X. Xiao, Y. Zhang, J. Wang, and H. Du, "An improved model predictive control scheme for the PWM rectifier-inverter system based on power-balancing mechanism," *IEEE Trans. Ind. Electron.*, vol. 63, no. 8, pp. 5197–5208, Aug. 2016.

[12] D. Zhou, J. Zhao, and Y. Liu, "Predictive torque control scheme for three-phase four-switch inverter-fed induction motor drives with DC-link voltages offset suppression," *IEEE Trans. Power Electron.*, vol. 30, no. 6, pp. 3309–3318, Jun. 2015.

[13] P. Cortes, J. Rodriguez, D. E. Quevedo, and C. Silva, "Predictive current control strategy with imposed load current spectrum," *IEEE Trans. Power Electron.*, vol. 23, no. 2, pp. 612–618, Mar. 2008.

[14] S. Kwak, S.-E. Kim, and J.-C. Park, "Predictive current control methods with reduced current errors and ripples for single-phase voltage source inverters," *IEEE Trans. Ind. Informat.*, vol. 11, no. 5, pp. 1006–1016, Oct. 2015.

[15] H. A. Young, M. A. Perez, and J. Rodriguez, "Analysis of finite-control-set model predictive current control with model parameter mismatch in a three-phase inverter," *IEEE Trans. Ind. Electron.*, vol. 63, no. 5, pp. 3100–3107, May 2016.

[16] S. Kwak, U.-C. Moon, and J.-C. Park, "Predictive-control-based direct power control with an adaptive parameter identification technique for improved AFE performance," *IEEE Trans. Power Electron.*, vol. 29, no. 11, pp. 6178–6187, Nov. 2014.

[17] J. Rodriguez, and P. Cortes, *Predictive Control of Power Converters and Electrical Drives*. Hoboken, NJ, USA: Wiley, 2012.

[18] T. Geyer, "Model predictive direct torque control: Derivation and analysis of the state-feedback control law," *IEEE Trans. Ind. Appl.*, vol. 49, no. 5, pp. 2146–2157, Sep. 2013.

[19] Y. Zhang and W. Xie, "Low complexity model predictive control—Single vector-based approach," *IEEE Trans. Power Electron.*, vol. 29, no. 10, pp. 5532–5541, Oct. 2014.

[20] Y. Zhang and H. Yang, "Two-vector-based model predictive torque control without weighting factors for induction motor drives," *IEEE Trans. Power Electron.*, vol. 31, no. 2, pp. 1381–1390, Feb. 2016.

[21] X. Shi, J. Zhu, L. Li, and D. D.-C. LU, "Low-complexity dual-vector-based predictive control of three-phase PWM Rectifiers without duty-cycle optimization," *IEEE Access*, vol. 8, pp. 77049–77059, 2020.

[22] J. Wang, H. Li, and L. Wang, "Direct power control system of three phase boost type PWM rectifiers," *Zhongguo Dianji Gongcheng Xuebao, Proc. Chin. Soc. Electr. Eng.*, vol. 26, no. 18, pp. 54–60, 2006.

[23] M. Malinowski, M. P. Kazmierkowski, S. Hansen, F. Blaabjerg, and G. D. Marques, "Virtual-flux-based direct power control of three-phase PWM rectifiers," *IEEE Trans. Ind. Appl.*, vol. 37, no. 4, pp. 1019–1027, Jul. 2001.

[24] X. Xiao, Y. Zhang, X. Song, T. Yildirim, and F. Zhang, "Virtual flux direct power control for PWM rectifiers based on an adaptive sliding mode observer," *IEEE Trans. Ind. Appl.*, vol. 54, no. 5, pp. 5196–5205, Sep./Oct. 2018.

[25] J. Fei and H. Wang, "Experimental investigation of recurrent neural network fractional-order sliding mode control of active power filter," *IEEE Trans. Circuits Syst. II, Exp. Briefs*, vol. 67, no. 11, pp. 2522–2526, Nov. 2020.

[26] J. Fei and Y. Chen, "Dynamic terminal sliding-mode control for single-phase active power filter using new feedback recurrent neural network," *IEEE Trans. Power Electron.*, vol. 35, no. 9, pp. 9904–9922, Sep. 2020.

[27] J. Fei and Z. Feng, "Fractional-order finite-time super-twisting sliding mode control of micro gyroscope based on double-loop fuzzy neural network," *IEEE Trans. Syst., Man, Cybern. Syst.*, early access, Mar. 25, 2020, doi: 10.1109/TSMC.2020.2979979.

[28] J. Liang, H. Wang, and Z. Yan, "Grid voltage sensorless model-based predictive power control of PWM rectifiers based on sliding mode virtual flux observer," *IEEE Access*, vol. 7, pp. 24007–24016, 2019.

[29] H. Yang, Y. Zhang, J. Liang, J. Gao, P. D. Walker, and N. Zhang, "Sliding-mode observer based voltage-sensorless model predictive power control of PWM rectifier under unbalanced grid conditions," *IEEE Trans. Ind. Electron.*, vol. 65, no. 7, pp. 5550–5560, Jul. 2018.

XIONG XIAO (Member, IEEE) was born in Hubei, China, in 1989. He received the Ph.D. degree in control science and engineering from the University of Science and Technology Beijing, Beijing, China, in 2017. He is currently a Postdoctoral Researcher with the Institute of Engineering Technology, University of Science and Technology Beijing. His research interests include synchronous motor drivers, power electronics, and nonlinear control theory research and its application in pulsewidth modulation rectifier–inverter systems.

YUJUAN WU was born in Shandong, China, in 1996. She received the bachelor's degree in automatic chemistry from the Shandong University of Science and Technology, Shandong, in 2018. She is currently pursuing the degree with the Institute of Engineering Technology, University of Science and Technology Beijing. Her research interests include synchronous motor drives and power electronics.

JIANTAO SU was born in Henan, China, in 1972. He is currently pursuing the Ph.D. degree with the School of Mechanical Engineering, University of Science and Technology Beijing. He is also a General Manager of Sci-Tech (Beijing) Technology Company Ltd. He is also a Specially Invited Expert of intelligent manufacturing by the China Machinery Industry Association. His research interests include intelligent manufacturing, intelligent equipment, advanced production arrangement.

YONGJUN ZHANG (Member, IEEE) was born in Shandong, China, in 1973. He received the M.Sc. and Ph.D. degrees in electrical engineering from the University of Science and Technology Beijing, Beijing, China, in 2002 and 2011, respectively. He is currently a Professor with the Engineering Research Institute, University of Science and Technology Beijing. His research interests include power electronics, motor drives, and their nonlinear control.

JINGZHI ZHOU is currently pursuing the master's degree in sports science with Zhejiang University, Hangzhou, China. Her research interests include human motion analysis, statistical analysis, and application of smart systems in sports science.